ACCOUNTS of chemical research

pubs.acs.org/accounts

Article

Use of Intramolecular Quinol Redox Couples to Facilitate the Catalytic Transformation of O_2 and O_2-Derived Species

Byron H. Farnum* and Christian R. Goldsmith*

Cite This: *Acc. Chem. Res.* 2025, 58, 101−112

Read Online

ACCESS | Metrics & More | Article Recommendations

CONSPECTUS: The redox reactivity of transition metal centers can be augmented by nearby redox-active inorganic or organic moieties. In some cases, these functional groups can even allow a metal center to participate in reactions that were previously inaccessible to both the metal center and the functional group by themselves. Our research groups have been synthesizing and characterizing coordination complexes with polydentate quinol-containing ligands. Quinol is capable of being reversibly oxidized by either one or two electrons to semiquinone or *para*-quinone, respectively. Functionally, quinol behaves much differently than phenol, even though the pK_a values of the first O−H bonds are nearly identical.

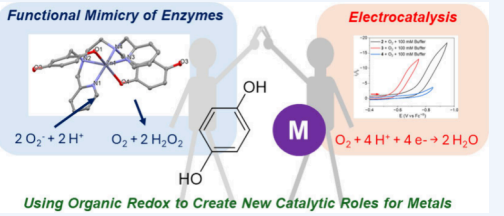

The redox activity of the quinol in the polydentate ligand can augment the abilities of bound redox-active metals to catalyze the dismutation of $O_2^{-\bullet}$ and H_2O_2. These complexes can thereby act as high-performing functional mimics of superoxide dismutase (SOD) and catalase (CAT) enzymes, which exclusively use redox-active metals to transfer electrons to and from these reactive oxygen species (ROS). The quinols augment the activity of redox-active metals by stabilizing higher-valent metal species, providing alternative redox partners for the oxidation and reduction of reactive oxygen species, and protecting the catalyst from destructive side reactions. The covalently attached quinols can even enable redox-inactive Zn(II) to catalyze the degradation of ROS. With the Zn(II)-containing SOD and CAT mimics, the organic redox couple entirely substitutes for the inorganic redox couples used by the enzymes. The ligand structure modulates the antioxidant activity, and thus far, we have found that compounds that have poor or negligible SOD activity can nonetheless behave as efficient CAT mimics.

Quinol-containing ligands have also been used to prepare electrocatalysts for dioxygen reduction, functionally mimicking the enzyme cytochrome c oxidase. The installation of quinols can boost electrocatalytic activity and even enable otherwise inactive ligand frameworks to support electrocatalysis. The quinols can also shift the product selectivity of O_2 reduction from H_2O_2 to H_2O without markedly increasing the effective overpotential. Distinct control of the coordination environment around the metal center allows the most successful of these catalysts to use economic and naturally abundant first-row transition metals such as iron and cobalt to selectively reduce O_2 to H_2O at low effective overpotentials. With iron, we have found that the electrocatalysts can enter the catalytic cycle as either an Fe(II) or Fe(III) species with no difference in turnover frequency. The entry point to the cycle, however, has a marked impact on the effective overpotential, with the Fe(III) species thus far being more efficient.

KEY REFERENCES

- Senft, L.; Moore, J. L.; Franke, A.; Fisher, K. R.; Scheitler, A.; Zahl, A.; Puchta, R.; Fehn, D.; Ison, S.; Sader, S.; Ivanović-Burmazović, I.; Goldsmith, C. R. Quinol-Containing Ligands Enable High Superoxide Dismutase Activity by Modulating Coordination Number, Charge, Oxidation States and Stability of Manganese Complexes throughout Redox Cycling. *Chem. Sci.* **2021**, *12*, 10483.[1] *The work describes how quinols impact the ability of manganese complexes with pyridylamine ligands to catalyze superoxide dismutation. The best of the catalysts is both highly active and relatively water-stable.*
- Ward, M. B.; Scheitler, A.; Yu, M.; Senft, L.; Zillmann, A. S.; Gorden, J. D.; Schwartz, D. D.; Ivanović-Burmazović, I.; Ison, S.; Sader, S.; Ivanović-Burmazović, I.; Goldsmith, C. R. Superoxide Dismutase Activity by a Zn(II) Complex with a Redox-Active Ligand. *Nature Chem.* **2018**, *10*, 1207.[2] *This work reports the first instance of zinc-catalyzed superoxide dismutation. It also documents the first example of a superoxide dismutase mimic with enhanced activity in phosphate buffer.*
- Karbalaei, S.; Franke, A.; Oppelt, J.; Aziz, T.; Jordan, A.; Pokkuluri, P. R.; Schwartz, D. D.; Ivanović-Burmazović, I.; Goldsmith, C. R. A Macrocyclic Quinol-Containing Ligand Enables High Catalase Activity even with a Redox-

Received: October 5, 2024
Revised: December 4, 2024
Accepted: December 5, 2024
Published: December 17, 2024

https://doi.org/10.1021/acs.accounts.4c00645
Acc. Chem. Res. 2025, 58, 101−112

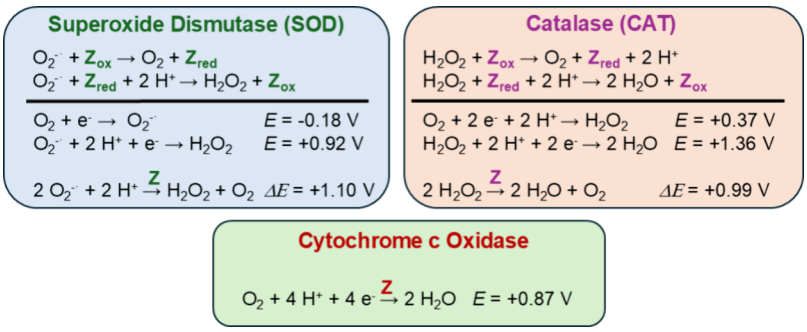

Figure 1. Selected enzymatic reactions and relevant reduction potentials relating to O_2 and O_2-derived reactive oxygen species. All potentials were reported in pH 7.0 water and are referenced to the normal hydrogen electrode.[6] Enzymatic species are abbreviated Z.

Inactive Metal at the Expense of the Ability to Mimic Superoxide Dismutase. *Chem. Sci.* **2023**, *14*, 9910.[3] *This report describes highly active catalase mimics containing either manganese, iron, or zinc. As with the prior report, the quinol in the ligand allows Zn(II) to catalyze a reaction that was previously thought to require a redox-active metal.*

- Obisesan, S. V.; Rose, C.; Farnum, B. H.; Goldsmith, C. R. A Co(II) Complex with a Covalently Attached Pendent Quinol Selectively Reduces O_2 to H_2O. *J. Am. Chem. Soc.* **2022**, *114*, 22826.[4] *This communication details how including a quinol in the ligand framework enables a previously unreactive Co(II) complex to serve as an electrocatalyst for O_2 reduction. The quinol complex is more selective for H_2O production than a phenolic analog.*

1. INTRODUCTION

Reactions involving O_2 and its partially reduced forms are of great relevance to the fields of health and energy. Aerobic organisms produce energy by reducing O_2 by four electrons to water, and partially reduced species, such as superoxide ($O_2^{-\bullet}$) and hydrogen peroxide (H_2O_2), are used as signaling agents for cellular processes such as apoptosis and gene expression.[5]

Despite their beneficial roles, $O_2^{-\bullet}$ and H_2O_2 can oxidize and damage biomolecules, and the overproduction and/or over-accumulation of these species can have adverse effects on health.[7−9] To limit the damage caused by these reactive oxygen species (ROS), cells produce a variety of antioxidants, including the metalloenzymes superoxide dismutase (SOD) and catalase (CAT). The active sites of SODs are diverse and have been documented to contain either mononuclear manganese, iron, nickel, and copper or binuclear copper/zinc.[10] CATs use either heme or binuclear manganese active sites to degrade H_2O_2.[11] Although SOD and CAT target different ROS and use dissimilar active sites, their dismutation of $O_2^{-\bullet}$ (SOD) and H_2O_2 (CAT) rely on similar strategies. Both classes of enzymes cycle between reduced and oxidized forms during catalysis (Figure 1). The reduced forms ($\mathbf{Z_{red}}$) reduce a ROS, whereas the oxidized forms ($\mathbf{Z_{ox}}$) oxidize the same ROS. During catalysis, SOD and CAT alternate between ROS reduction and ROS oxidation steps. The activities of these enzymes have inspired efforts to develop small molecule mimics that could supplement the body's defenses against oxidative stress, but these efforts have been stymied by several factors, including poor stability and attenuated activity under physiologically relevant conditions.[12−35]

With respect to O_2 reduction to water, nature uses cytochrome c oxidase to achieve this complex $4e^-/4H^+$ reaction. The active site of the enzyme contains multiple redox-active units, including an iron porphyrin, a histidine-bound copper center, and a proximal tyrosine.[36,37] All of these units work in concert to manage proton- and electron-transfer reactions to avoid partial reduction of O_2 to $O_2^{-\bullet}$ and H_2O_2 (Figure 1).[37,38] Energy-related technologies such as metal-air batteries and hydrogen fuel cells also rely on the oxygen reduction reaction (ORR). Within these applications, partial reduction of O_2 to a ROS is arguably even more problematic than it is for physiology since H_2O_2 and $O_2^{-\bullet}$ will corrode the components in these devices without providing any benefits analogous to those found in biology. This said, there is significant interest in the development of fuel cells which use H_2O_2 instead of H_2 as the fuel source.[39−42] The O_2 reduction that occurs at the cathodes of metal-air batteries and hydrogen fuel cells requires an electrocatalyst that can efficiently promote the full four-electron reduction of O_2 and avoid the production of ROS.

Most cathode electrocatalysts for these devices contain platinum, which is both expensive and naturally scarce.[43] The lesser cost and higher natural abundance of first-row transition metals, such as iron, have motivated attempts to develop electrocatalysts using these elements.[44−47] Unfortunately, first-row transition metal electrocatalysts for the ORR tend to either preferentially catalyze two-electron reduction of O_2 to H_2O_2 or operate at extremely high effective overpotentials.[43,46−64]

1.A. Quinols as Redox-Active Organic Components in Catalysts

1,4-Hydroquinones (quinols) can potentially lose two electrons and two protons as they oxidize/deprotonate to stable *para*-quinones (Scheme 1). The product of one-electron oxidation, semiquinone, is also stable for an organic radical.[65] Quinols and/or their oxidized forms can therefore form the basis for both two- and one-electron redox couples that could supplement the redox chemistry of first-row transition metals toward catalytic reactions. Derivatives of quinols and *para*-quinones, such as ubiquinone, have been amply documented to participate in biological electron transfer reactions.[66,67] In small molecule catalysis, quinols and *para*-quinones have been used as electron proton transfer mediators (EPTMs). Stahl and co-workers were able to shift the product selectivity of cobalt-catalyzed ORR from H_2O_2 to water by adding excess free quinol.[68] Machan and co-workers later did the same for manganese-catalyzed ORR.[69]

Despite their successes as EPTM additives, quinol/*para*-quinone groups have rarely been directly installed into the polydentate ligands of molecular catalysts. Rare examples include a Pd(II)-containing catalyst for 1,3-diene diacetoxylation and a Pd(0)-containing catalyst for dioxygen reduction.[70,71] Singha et al. installed phenols and quinols onto a porphyrin framework and used iron complexes with these ligands as electrocatalysts for ORR.[51] The incorporation of a

https://doi.org/10.1021/acs.accounts.4c00645
Acc. Chem. Res. 2025, 58, 101−112

Scheme 1. Overview of Possible Acid/Base and Redox Reactions Involving Quinols[a]

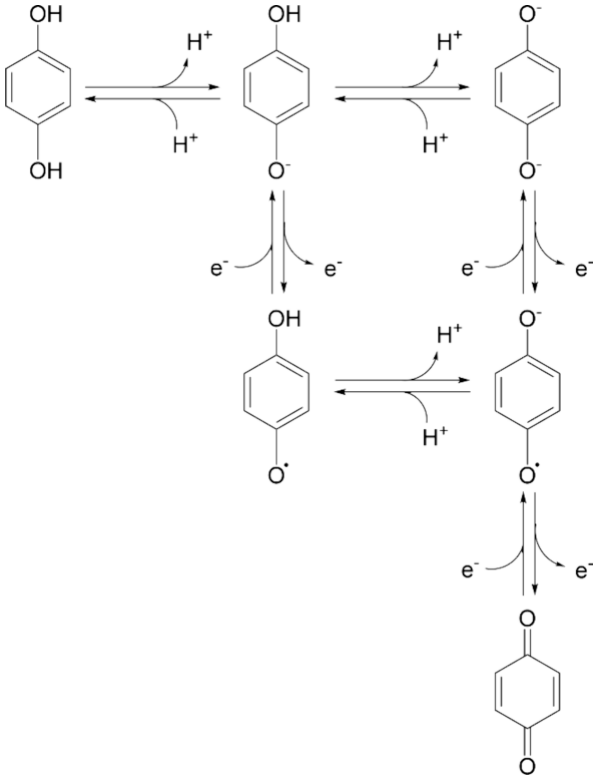

[a]For clarity, possible proton-coupled electron transfer reactions are not shown.

quinol, however, did not have a noticeable impact on the product selectivity, and the quinolic and phenolic complexes had similar rates of activity. Iron-porphyrin complexes have historically promoted the reduction of O_2 to water at high effective overpotentials, so water would be the expected product even without the quinol.[48−50,55,56,72]

1.B. Initial Development of Polydentate Quinol-Containing Ligands

Our initial interest in quinols was motivated by using their redox-controlled lability to prepare magnetic resonance imaging (MRI) contrast agents that could respond to H_2O_2. The reduced form can readily deprotonate to an anionic quinolate, which can coordinate metal ions tightly (Scheme 1); the two-electron oxidized *para*-quinone form, conversely, is a poor ligand. We prepared a series of polydentate ligands with either one or two quinols, including H_2qp1, H_4qp2, H_2qp3, and H_4qp4 (Scheme 2), and prepared manganese- and iron-containing MRI contrast agents with H_2qp1, H_4qp2, and H_4qp4.[73−76] Each of the MRI contrast agents could successfully detect H_2O_2 via an increase in its T_1-weighted relaxivity. For the manganese complexes, this increase results from better aquation; water molecules can coordinate to the metal center instead of the erstwhile quinol.[74−76] With iron, the response is instead correlated to the oxidation of the metal center from Fe(II) to Fe(III).[73]

Our interest in using these ligands and their complexes for other applications originated from an oddity that we noted during the MRI studies. Adding excess H_2O_2 to the Mn(II) complexes with H_2qp1 and H_4qp2 never oxidized more than ∼70% of the quinols.[75,76] No matter how much H_2O_2 was added or how long the reaction was allowed to proceed, the same proportion of quinol was oxidized to *para*-quinone. It appeared that we were reaching the same equilibrium position for these reactions which would imply that the oxidized (*para*-quinone) complexes had a means of reducing back to their original (quinol) forms. If the reduction of these complexes used an ROS as the reductant, the overall reactivity would resemble those of SOD and CAT (Figure 1).

2. FUNCTIONAL MIMICS OF SUPEROXIDE DISMUTASE

2.A. Manganese-Containing Complexes

The Mn(II) complexes with H_2qp1 and H_4qp2 both have ligand-derived redox features with $E_{1/2}$ values of approximately 0.3 V vs NHE,[75,76] which is approximately midway between the potentials for the oxidation (−0.18 V) and reduction (+0.92 V) of superoxide.[77,78] SODs themselves usually have $E_{1/2}$ values close to this value.[79] Preliminary antioxidant assays of $[Mn^{II}(H_2qp1)(MeCN)](OTf)_2$ (**1**, OTf^- = triflate) and $[Mn^{II}(H_4qp2)Br_2]$ (**2**) suggested that the complexes could behave as functional mimics of SOD.[75,76] The xanthine/xanthine oxidase/lucigenin assay[80,81] predicted that the activities of **1** and **2** were slightly inferior to that of $[Mn^{II}(Hptp1)(MeCN)](OTf)_2$ (**3**), which features a phenolic ligand similar to H_2qp1 (Scheme 2).[75] Complex **3** dismutates $O_2^{-\bullet}$ through primarily an outer-sphere mechanism with a rate constant that is much lower than the $>10^8$ M^{-1} s^{-1} value predicted by the assay (Table 1).[82]

Subsequent stopped-flow kinetics analysis of the direct reactions between KO_2 and either **1** or **2** confirm that both manganese compounds are functional SOD mimics (Table 1).[1] The metal-free H_2qp1 and H_4qp2 ligands are unable to catalyze $O_2^{-\bullet}$ dismutation by themselves.[1,2] Complex **1** is more active in

Scheme 2. Quinolic and Phenolic Polydentate Ligands Discussed in This Account

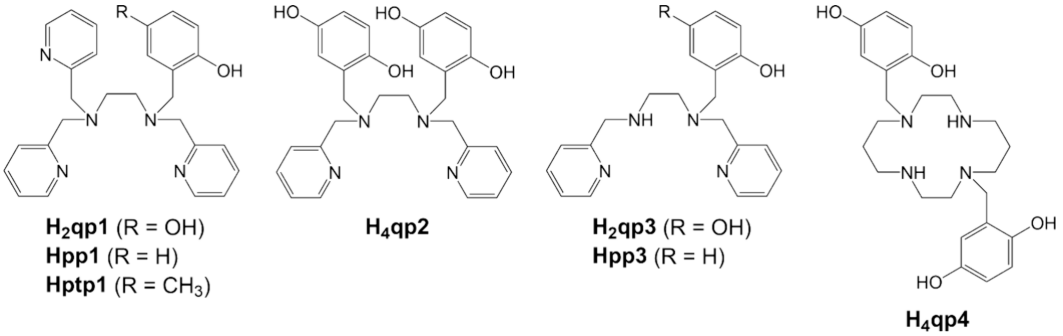

https://doi.org/10.1021/acs.accounts.4c00645
Acc. Chem. Res. 2025, 58, 101−112

Table 1. Measures of SOD Mimicry for Metal Complexes with Quinolic and Phenolic Ligands[a]

catalyst	IC_{50}[b] (nM)	k_{cat}[c] (M^{-1} s^{-1}) HEPES/MOPS, pH 7.4	k_{cat}[c] (M^{-1} s^{-1}) HEPES/MOPS, pH 7.8	k_{cat}[c] (M^{-1} s^{-1}) HEPES/MOPS, pH 8.1	k_{cat}[c] (M^{-1} s^{-1}) phosphate, pH 7.4
$[Mn^{II}(H_2qp1)(MeCN)]^{2+}$ (**1**)	11.3[d]	9.7×10^7[e]	N.D.	2.2×10^7[e]	8.0×10^6[e]
$[Mn^{II}(H_4qp2)Br_2]$ (**2**)	18.2[f]	1.2×10^7[e]	N.D.	9.6×10^6[e]	1.0×10^7[e]
$[Mn^{II}(Hptp1)(MeCN)]^{2+}$ (**3**)	7.7[d]	3.6×10^6[g]	N.D.	6.2×10^5[g]	1.1×10^6[g]
$[Mn^{II}(H_3qp4)]^{+}$ (**4**)	15[h]	6.0×10^6[h,i]	4.5×10^6[h,i]	N.D.	2.9×10^6[h]
$[Fe^{II}(H_3qp4)]^{+}$ (**5**)	21[h]	inactive[h,i]	inactive[h,i]	N.D.	inactive[h]
$[Zn^{II}(H_2qp1)(OTf)]^{+}$ (**6**)	16.8[j]	3.4×10^6[j]	N.D.	4.7×10^6[j]	1.9×10^7[j]
$[Zn^{II}(H_4qp2)]^{2+}$ (**7**)	24.4[k]	1.6×10^7[i,k]	4.9×10^7[i,k]	N.D.	2.5×10^7[k]
$[Zn^{II}(H_2qp3)(H_2O)]^{2+}$ (**8**)	27.1[k]	inactive[i,k]	inactive[i,k]	N.D.	inactive[k]
$[Zn^{II}(H_3qp4)]^{+}$ (**9**)	515[h]	inactive[h]	inactive[h]	N.D.	inactive[h]
$[Zn^{II}(Hpp1)]^{2+}$ (**10**)	N.D.	inactive[i,l]	N.D.	N.D.	N.D.

[a]All compounds except **2** contained triflate (OTf^-) as the counteranion. [b]Calculated from assays. Superoxide is generated from reactions between hypoxanthine and xanthine oxidase in 50 mM Tris-HCl buffered to pH 8.0 and detected using the chemiluminescent probe lucigenin. The reported IC_{50} is the concentration of SOD mimic that eliminates half the lucigenin response. [c]Calculated from stopped-flow kinetics data from direct reactions between KO_2 and the SOD mimic. HEPES/MOPS data are collected in 60 mM HEPES unless otherwise noted. All phosphate data are collected in 50 mM phosphate. The low pK_a of HO_2 (4.8) ensures that superoxide is predominantly $O_2^{-\bullet}$ at pH 7.4 and above. [d]Reference 75. [e]Reference 1. [f]Reference 76. [g]Reference 82. [h]Reference 3. [i]Collected in 60 mM 3-(*N*-morpholino)propanesulfonic acid (MOPS). [j]Reference 2. [k]Reference 83. [l]Reference 84.

Scheme 3. Proposed Mechanisms of $O_2^{-\bullet}$ Dismutation Catalyzed by 1 and 2[a]

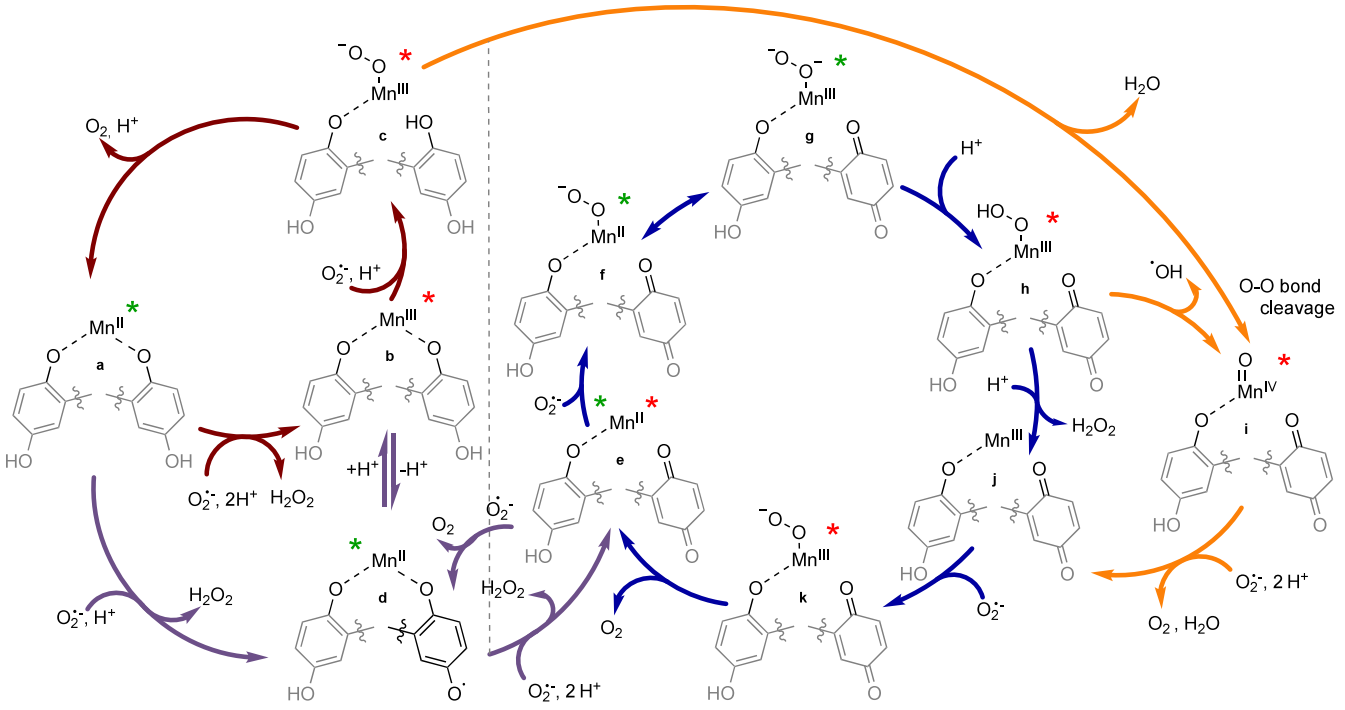

[a]The two quinol groups of H_4qp2 and the metal center are shown with the rest of the complex omitted for clarity. For species derived from **1**, the leftmost quinol is replaced by a pyridine ring from the H_2qp1 ligand. Intermediates marked with * were observed by CSI-MS for **1**; those marked with * were instead detected for **2**. Mn−O−O^- species contain superoxide ligands, whereas the Mn−O^-−O^- species contain peroxide. This graphic was reused with permission from ref 1. Copyright 2021 Royal Society of Chemistry.

aqueous solutions with sulfonate-based buffers such as 4-(2-hydroxyethyl)-1-piperazineethanesulfonic acid (HEPES). The k_{cat} rate constant for overall superoxide dismutation in 50 mM HEPES buffered to pH 7.4 is high for an SOD mimic—and much higher than it is for the phenolic analog **3** - but is exceeded by those of the most active manganese-porphyrin and manganese-pentaazamacrocyclic catalysts for $O_2^{-\bullet}$ degradation.[24,31−34] Potentiometric pH titration data, however, suggest that **1** is more water-stable than these other catalysts.[24,31,32] Much like several other highly active manganese-containing SOD mimics, **1** loses most of its activity when superoxide dismutation is assessed under more basic conditions or in phosphate solution.[20,29,82] Phosphate is proposed to attenuate the activity by competing with $O_2^{-\bullet}$ for coordination sites on the metal ion.[20]

The diquinolic **2** is less active than **1** but does not lose significant activity in the presence of phosphate. Complex **2** differs from **1** in that the major species at pH ≥ 7.4 is neutral

https://doi.org/10.1021/acs.accounts.4c00645
Acc. Chem. Res. 2025, 58, 101−112

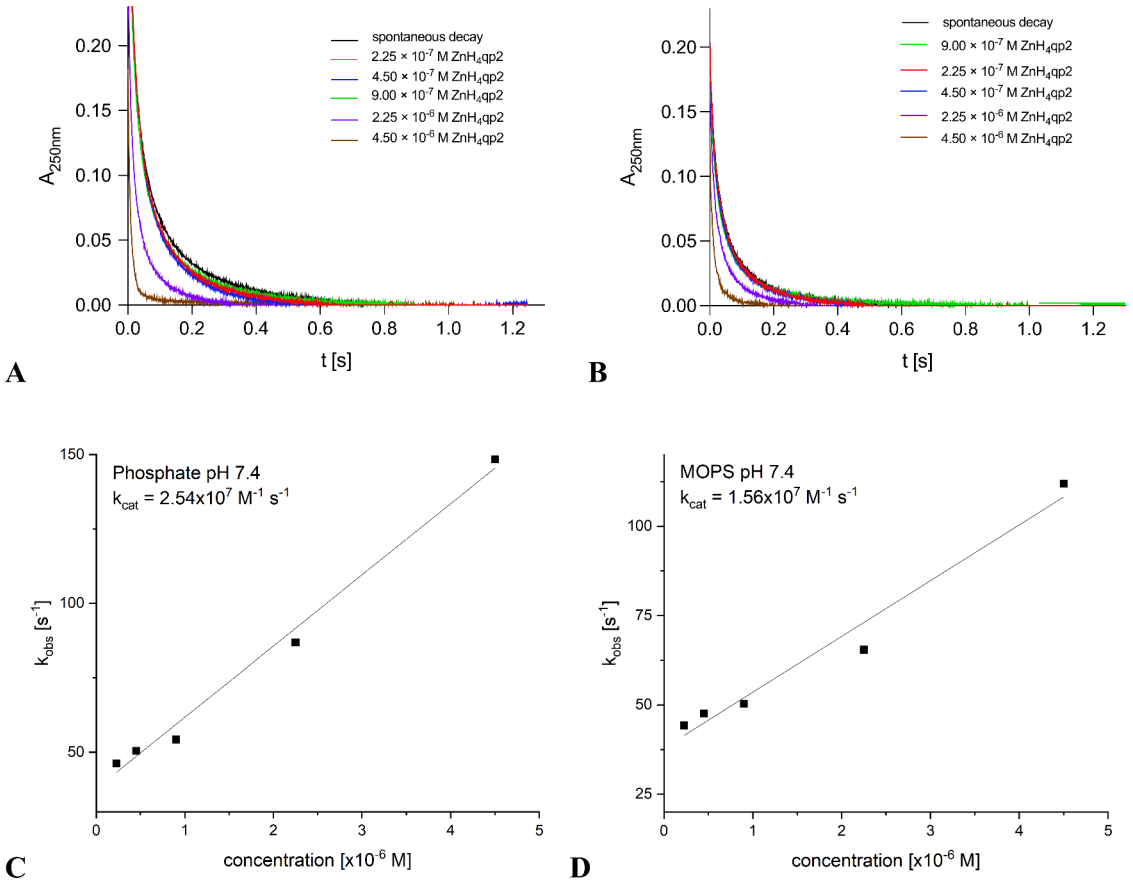

Figure 2. Kinetic traces of $O_2^{-\bullet}$ decomposition catalyzed by **7**. The concentration of the $O_2^{-\bullet}$ is monitored by the intensity of its band at 250 nm. (A) Data taken in 50 mM phosphate buffer, pH 7.4 ionic strength of 150 mM. The starting concentration of superoxide is 1.5×10^{-4} M. (B) Data taken in 60 mM MOPS buffer, pH 7.4 ionic strength of 150 mM. The starting concentration of superoxide is 9×10^{-5} M. (C) Plot of k_{cat} values from A vs [**7**] for the pH 7.4 phosphate data. (D) Plot of k_{cat} values from B vs [**7**] for the pH 7.4 MOPS data. This graphic was reused with permission from ref 83. Copyright 2022 American Chemical Society.

($[Mn^{II}(H_2qp2)]$) rather than cationic ($[Mn^{II}(Hqp1)]^+$) due to the ability of both quinols in H_4qp2 to singly deprotonate, yielding H_2qp2^{2-}.[1,76] The lower positive charge on **2** impedes its ability to attract and coordinate anionic species. This in turn, both lowers the rate constants for $O_2^{-\bullet}$ degradation and largely eliminates phosphate inhibition.

Mn(II) and Fe(II) complexes with H_4qp4, which is a macrocyclic rather than linear ligand, were also tested as SOD mimics. Although the xanthine/xanthine oxidase/lucigenin assay suggests that both compounds could catalytically degrade superoxide, stopped-flow kinetics experiments again determine that their actual activities are less than what these assays predict (Table 1).[3] The Mn(II) complex, $[Mn^{II}(H_3qp4)](OTf)$ (**4**), directly reacts with $O_2^{-\bullet}$ but with a k_{cat} less than that of **1** or **2**. The iron analog $[Fe^{II}(H_3qp4)](OTf)$ (**5**) is completely inactive as a SOD mimic. Although the assay results frequently overestimate the catalytic activity of our SOD mimics and generally do a poor job of predicting relative activities (Table 1), this represents one of two instances in our research where the assay suggests activity for an entirely inactive complex.

The mechanism of $O_2^{-\bullet}$ degradation by **1** and **2** was probed with several techniques including cryo-ionization mass spectrometry (cryo-MS) and low temperature UV/vis and electron paramagnetic resonance (EPR) spectroscopies.[1] The results suggest that both the metals and the organic ligands cycle through different oxidation states during catalysis (Scheme 3). Cryo-MS of reactions occurring in MeCN at −40 °C with solid KO_2 detects Mn(II) and Mn(III) complexes with the quinol (H_2qp1, H_4qp2) and mono-*para*-quinone forms (qp1, H_2qp2) of the two ligands as well as a Mn(IV)-oxo species with H_2qp2. The identity of the Mn(IV)-H_2qp2 species was supported by EPR of a freeze-quenched sample of **2** reacting with KO_2. These experiments also found evidence for Mn(II)-superoxo, Mn(III)-superoxo, Mn(III)-peroxo, and Mn(III)-hydroperoxo complexes, providing evidence for inner-sphere pathways of $O_2^{-\bullet}$ oxidation and/or reduction for both **1** and **2**. The presence of semiquinone radicals was supported by low temperature UV/vis experiments. When **2** reacts with KO_2 in MeCN at −40 °C, absorption bands develop at 422 and 448 nm; these are consistent with semiquinone radical anions.[85,86]

The quinols are proposed to assist in the catalysis in several ways.[1] First, the abilities of the quinols to deprotonate to anionic groups and to transfer electrons should stabilize the manganese in higher oxidation states. Second, the quinols themselves can act as the redox partners for $O_2^{-\bullet}$, with the organic redox cycles likely being more important for **1** than **2** due to its having one fewer possible quinolate to promote metal-centered redox. Third, the quinols can protect the catalyst against side reactions with ROS and metal-based oxidants generated *in situ* that would otherwise destroy the ligand and halt efficient catalysis.

2.B. Zinc-Containing Complexes

The fact that the $E_{1/2}$ values that were reminiscent of the enzymatic SOD redox potentials derive from the ligands led us

https://doi.org/10.1021/acs.accounts.4c00645
Acc. Chem. Res. 2025, 58, 101−112

Scheme 4. Calculated Mechanism for the Dismutation of $O_2^{-\bullet}$ by 6[84,a]

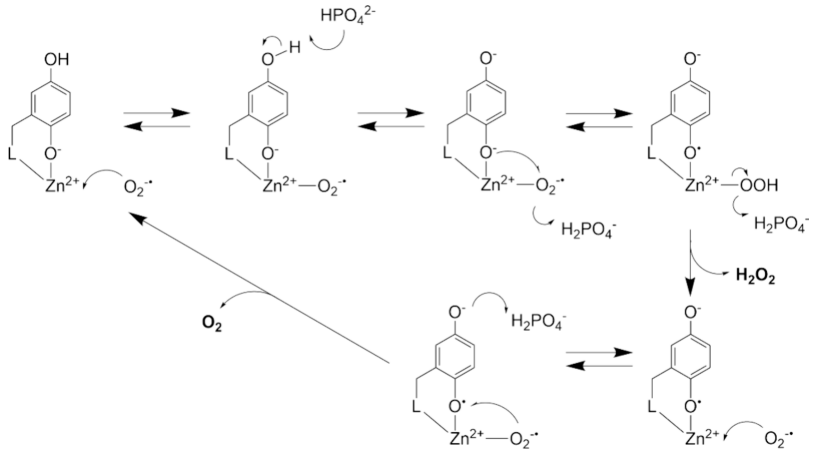

[a]The H_2qp1 ligand is abbreviated to just the quinol-derived groups. Minor reactions that would account for the formation of the *para*-quinone species $[Zn^{II}(qp1)]^{2+}$ are not shown.

to hypothesize that SOD activity could be achieved with quinolic complexes with redox-inactive metal ions. We consequently prepared Zn(II) compounds with H_2qp1, H_4qp2, H_2qp3, and H_4qp4 and assessed their reactivity with $O_2^{-\bullet}$ with stopped-flow kinetics (Table 1). $[Zn^{II}(H_2qp1)(OTf)](OTf)$ (**6**) and $[Zn^{II}(H_4qp2)](OTf)_2$ (**7**) catalyzed $O_2^{-\bullet}$ dismutation, but $[Zn^{II}(H_2qp3)(H_2O)](OTf)_2$ (**8**) and $[Zn^{II}(H_3qp4)](OTf)$ (**9**) are inactive.[2,3,83] The catalytic activities of **6** and **7** confirm that quinol-derived redox couples can indeed substitute for transition metal redox activity in SOD mimicry. Much like **5**, **8** gave rise to a false positive on the assay used to screen SOD activity.[83] Complex **7** is more active than **6**, with the differences being larger in sulfonate-derived buffers.

Complexes **6** and **7** are further notable for exhibiting phosphate-enhanced, rather than phosphate-inhibited, catalysis (Figure 2).[2,83] We proposed that the lack of inhibition was a consequence of phosphate not binding to Zn(II) as avidly as Mn(II) and Mn(III); this was later supported by a computational analysis of the reactivity of **6**.[84] The improvement in the activity in phosphate relative to sulfonate buffers was proposed to result from more efficient proton transfer between the buffer and the cationic species on the catalytic cycle. At pH 7.4, phosphate exists as a mixture of two negatively charged species ($H_2PO_4^-$ and HPO_4^{2-}), whereas only the conjugate bases for HEPES and MOPS are anionic.

The inabilities of **8** and **9** to catalyze $O_2^{-\bullet}$ decomposition result from different phenomena. Complex **8** features the pentadentate H_2qp3 ligand, which coordinates to metal ions much more weakly than H_2qp1, H_4qp2, and H_4qp4.[3,73,74,83] Using mass spectrometry, we determined that the ligand dissociates from the metal ion upon oxidation. Given that free H_2qp1 and H_4qp2 could not act as catalysts, the dissociation of oxidized H_2qp3 from the metal center in **8** would be anticipated to halt SOD mimicry. The rationale for the lack of activity for the extremely water-stable **9** is not fully understood, but it is likely related to the poor SOD mimicry observed for the other H_4qp4 complexes **4** and **5**. Our computational analysis of **6** suggests that $O_2^{-\bullet}$ needs to coordinate *cis* to a metal-bound quinolate in order for dismutation to proceed efficiently,[84] and it may be that the H_4qp4 ligand framework discourages such conformations for the manganese, iron, and zinc complexes.

The mechanism of zinc-catalyzed SOD mimicry was probed both experimentally and theoretically. The results confirm that the quinolic portions of the ligands cycle through different oxidation states during catalysis (Scheme 4). Reaction with one equiv of $O_2^{-\bullet}$ would be anticipated to generate a Zn(II)-semiquinone radical and HOO^-. When either **6** or **7** reacts with one equiv of a noncoordinating base (Et_3N) and one equiv of a one-electron oxidant ($Ag^I(OTf)$), we observe species with the anticipated EPR spectra.[2,83] In reactions between KO_2 and **7**, we directly observe UV/vis evidence for semiquinone species during catalysis.[83] The computational analysis of the reactivity of **6** suggests that inner-sphere pathways for $O_2^{-\bullet}$ degradation are operable,[84] but we were unable to fully support this with experimental evidence. Although mass spectrometry detects an m/z signature that is consistent with a Zn(II)-OOH species for **6**, we were unable to corroborate its identity with isotopic labeling,[2] and analogous species are not observed for **7**.[83] Our calculations suggest that the ability of the second hydroxy group on the quinol to deprotonate is essential for the stabilization of key reactive intermediates.[84] In particular, deprotonation of the nonmetal-bound OH by buffer enables the reaction to proceed through a lower energy semiquinolate anion, facilitating electron transfer from the quinolic portion of the ligand to the metal-bound superoxide. This may explain why **6** and **7** exhibit faster rates of catalysis under more basic conditions (Table 1).[2,83] The phenolic analog of **6**, $[Zn^{II}(Hpp1)](OTf)_2$ (**10**), is unable to catalyze the dismutation of $O_2^{-\bullet}$, corroborating the role of the nonmetal bound OH in catalysis.[84] The reactivity is predicted to rely mostly on the first one-electron redox couple; Zn(II)-*para*-quinone species are not predicted to be major oxidants. Although *para*-quinone species are observed among the end-products of superoxide dismutation catalyzed by both **6** and **7**,[2,83] these are currently believed to result from minor pathways.

3. FUNCTIONAL MIMICS OF CATALASE

Despite their near total inability to mimic SOD, the H_4qp4 complexes are still potent antioxidants since all three compounds catalyze the dismutation of H_2O_2.[3] We initially synthesized **4** and **5** to be MRI contrast agent sensors for H_2O_2.[73,74] These sensors differ from **1** and **2** in that large excesses of H_2O_2 do not immediately activate the MRI response; instead, both responses display induction periods that shorten as

https://doi.org/10.1021/acs.accounts.4c00645
Acc. Chem. Res. 2025, 58, 101−112

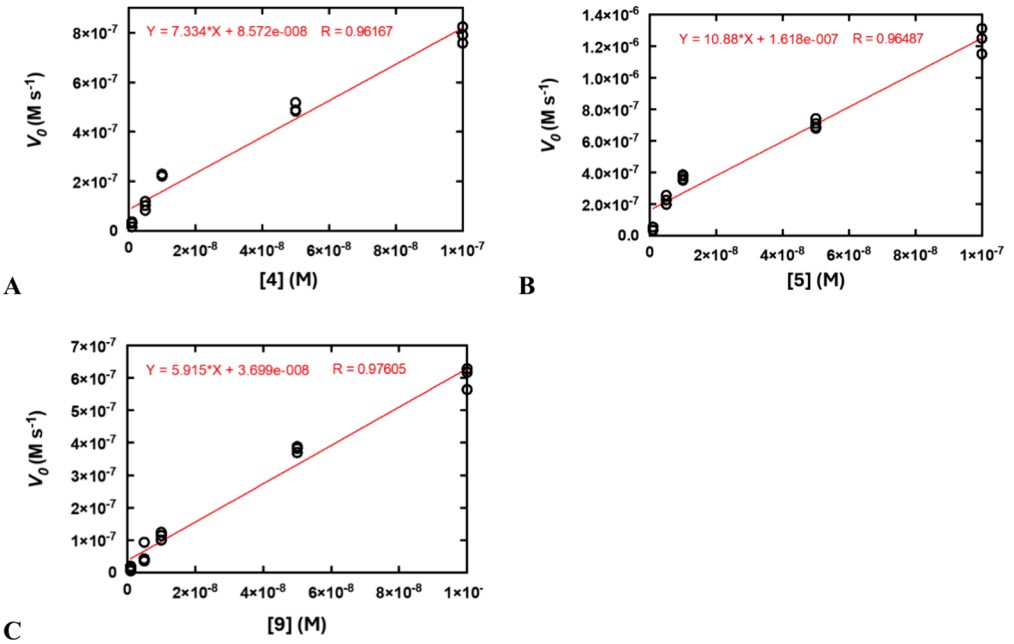

Figure 3. Plots of the initial rates of O_2 generation (v_o) vs concentration of catalyst. All reactions were run at 25 °C in 50 mM tris(hydroxymethyl)aminomethane (Tris) buffered to pH 7.2 with initial concentrations of 10 mM H_2O_2. The k_2 values on Table 2 were calculated by dividing the slopes of the shown linear fits by the concentration of H_2O_2 (0.010 M) and multiplying by two to account for the reaction stoichiometry (2 $H_2O_2 \rightarrow O_2 + 2\ H_2O$). (A) Data for **4**. (B) Data for **5**. (C) Data for **9**. This graphic was slightly adapted with permission from ref 3. Copyright 2023 Royal Society of Chemistry.

the amount of added H_2O_2 is decreased. From these unusual kinetics, we hypothesized that an intermediate formed from the initial reaction with H_2O_2 can either oxidize the ligand and provide the MRI response or oxidize another equiv of H_2O_2 to O_2 and revert the metal complex to its reduced form. It is only when most of the H_2O_2 has been depleted that the ligand oxidation becomes noticeable and the MRI response fully manifests. We supported this hypothesis by confirming O_2 evolution from the reactions between the H_4qp4 complexes and H_2O_2 (Figure 3).[3] Given that Zn(II) complexes with polydentate quinol ligands could act as SOD mimics, we also tested **9** and determined that it too was a CAT mimic. Although a redox-active metal is not required for CAT mimicry, coordinated metal ions are still essential. H_4qp4 by itself cannot catalyze H_2O_2 decomposition.

Complexes **4**, **5**, and **9** display exceptional reactivity with H_2O_2 as assessed by both their second-order rate constants (k_2) and turnover numbers (TON, Table 2).[3] Direct comparison with other CAT mimics is not always straightforward since these catalysts have been evaluated several different ways, with temperature, solution, and the method of following H_2O_2 degradation/O_2 production being possible variables. The rate constants for the H_4qp4 complexes are possibly only exceeded by an Fe(III) complex with a fluorinated corrole reported by Mahammad and Gross.[19] The k_2 of 4300 M^{-1} s^{-1} for the reaction between this compound and H_2O_2, however, was measured at 37 °C pH 7.4 phosphate buffer, rather than the 25 °C pH 7.2 Tris buffer used for our measurements.[3] Further, Mahammad and Gross determined k_2 from UV/vis measurements that followed the decomposition of H_2O_2.[19] This UV/vis technique sometimes overestimates the rate constants for CAT mimics,[14] and we find that this is the case for our own catalysts.[3,73,74]

Table 2. k_2 Rate Constants and Turnover Numbers (TON) Calculated from Oxygraphic Data for the H_4qp4 Complexes[a]

catalyst	k_2 (M^{-1} s^{-1})	TON
$[Mn^{II}(H_3qp4)]^+$ (**4**)	1.5×10^3	80
$[Fe^{II}(H_3qp4)]^+$ (**5**)	2.2×10^3	130
$[Zn^{II}(H_3qp4)]^+$ (**9**)	1.2×10^3	51

[a]All complexes used in these studies contain OTf^- counteranions. All reactions were run in 25 °C 50 mM Tris solutions buffered to pH 7.2. See ref 3 for more details.

The TON values for the H_4qp4 complexes exceed those of other CAT mimics. Until recently, the best TON had been 12.54 for a manganese-porphyrin complex.[14] Over the past few years, however, Green's group has reported CAT mimics with higher TON values.[17,35] The best of the catalysts are manganese complexes with pyridinophane ligands, and with judicious synthetic modification, the TON can reach 37.[17] Much like H_4qp4, the pyridinophane derivatives are macrocyclic, and we hypothesize that the high activities associated with both classes of ligand at least partly result from the high aqueous stabilities of their metal complexes.[3,17,73,74] The H_4q4 complexes also display little peroxidase activity.[3] Since such side reactivity could be directed toward the organic components of the CAT mimic,[87] the lack of peroxidase activity renders **4**, **5**, and **9** oxidatively robust, further prolonging catalysis.

Although it is the least active of the three H_4qp4-containing CAT mimics, the Zn(II) complex **9** is unique in that it promotes H_2O_2 dismutation without a redox-active metal ion.[3] As with the aforementioned SOD activity, quinol-related redox couples can therefore replace metal-derived ones in the catalytic degradation of ROS. Although the mechanism(s) of catalysis are still under investigation, **4** and **5** appear to rely more heavily on metal redox couples for catalysis (Scheme 5); these compounds differ from **9** in that we do not observe substantial ligand oxidation until late in catalysis.[3,73,74] EPR data also suggest that the Mn(II) and

https://doi.org/10.1021/acs.accounts.4c00645
Acc. Chem. Res. 2025, 58, 101−112

Scheme 5. Proposed Mechanisms for CAT Mimicry by H_4qp4 Complexes[a]

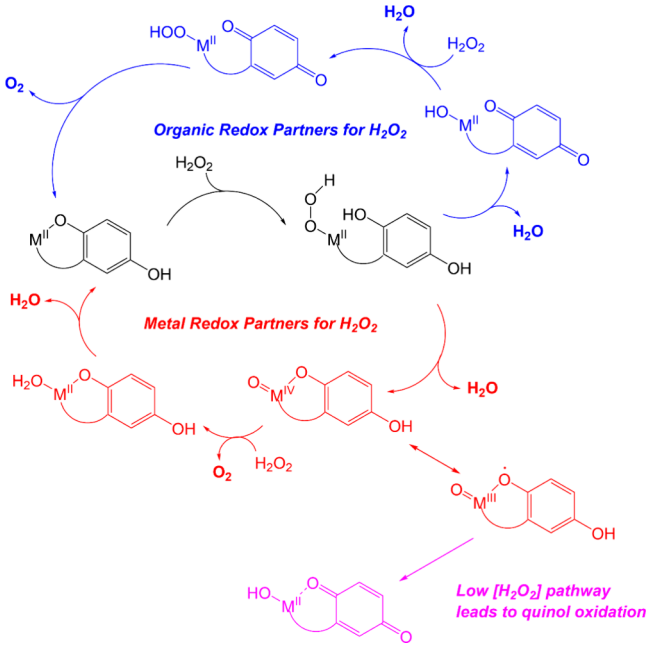

[a]The Zn(II) complex **9** is proposed to proceed through the organic redox cycle whereas **4** and **5** are proposed to mostly use the metal redox cycle, with ligand oxidation only occurring as the H_2O_2 depletes. This graphic was adapted with permission from ref 3. Copyright 2023 Royal Society of Chemistry.

Fe(II) in **4** and **5** oxidize.[3] The CAT mimicry of coordination complexes with linear quinol-containing ligands is currently being investigated.

4. FUNCTIONAL MIMICS OF CYTOCHROME C OXIDASE/ELECTROCATALYSTS FOR DIOXYGEN REDUCTION

Given Stahl and Machan's successes in using quinols to shift the favored product of ORR from H_2O_2 to H_2O,[68,69] we were curious as to whether covalently attaching such groups to the catalytic framework could provide similar or better benefits. Thus, we tested Co(II), Fe(II), and Fe(III) complexes with H_2qp1, H_4qp2, and H_2qp3 as electrocatalysts for the ORR in acetonitrile solvent (Table 3).[4,88] The H_4qp4 complex **5** reacts too slowly with O_2 to be an effective catalyst.[73] Complexes with the phenolic analogs Hpp1 and Hpp3 (Scheme 1) were also analyzed for comparative purposes.

Initial work in this area focused on cobalt catalysts. Although the Co(II) complex with *N*,*N*,*N*′-tris(2-pyridinylmethyl)-1,2-ethanediamine (trispicen) is electrocatalytically inactive, compounds with H_2qp1 (**10**) and Hpp1 (**11**) are both active (Table 3).[4] The quinolic **10** and the phenolic **11** have nearly identical effective overpotentials (η_{eff}) and activities, as assessed by their TOF_{max} values, but **10** is noticeably more selective for the four-electron reduction of O_2 to water. The results suggest that the quinol primarily impacts the product-determining steps and demonstrate that redox-active groups can improve the product selectivity of ORR for water without increasing η_{eff}. Adding 2.5 mM free quinol to the reaction mixtures was found to improve the yields of water from 61% to 89% for **10** and from 11% to 61% for **11**. The results suggest to us that covalently incorporating the quinol into the catalyst framework is a more efficient way to improve product selectivity than adding free quinol as an EPTM.

Subsequent work with iron complexes focused on establishing structure−function relationships and investigating alternative entry points into the catalytic cycle.[88] To our initial surprise, the Fe(II) complex with H_2qp1 (**12**) is inactive as an electrocatalyst for ORR, but Fe(II) and Fe(III) complexes with H_4qp2 and the lower dentate H_2qp3 are all active (Table 3). The inability of **12** to catalyze the ORR is attributed to its high M(III/II) reduction potential and subsequently low overpotential. The additional pyridine in the ligand structure (Scheme 1) renders this potential more positive and consequently slows the reaction with O_2, which would generate an Fe(III)-superoxo species. Both of the Fe(II) electrocatalysts with H_4qp2 (**13**) and H_2qp3 (**14**) have much higher TOF_{max} values and better selectivities for water than the cobalt complexes **10** and **11**, albeit with more positive η_{eff} (Table 3).[4,88] The Fe(III) complexes with both ligands are also electrocatalysts, but the activity of the H_4qp2 complex (**15**) could not be reliably determined due to substantial heterogeneous behavior, which we attribute to catalyst deposition onto the electrode.[88] The Fe(III) complex with H_2qp3 (**16**), however, displays better solubility and is more amenable to study. Although the reactivity of **16** resembles that of its Fe(II) analog **14** in most aspects, the η_{eff} is lower by 50 mV. The difference in potential is the result of **16** being reduced at the Fe(III) state, whereas **14** is reduced at the Fe(III)-$O_2^{-\bullet}$ state. The results suggest that entering the catalytic cycle through the Fe(III) species is more efficient and more generally, that changing the entry point is a viable strategy for improving the efficiency of electrocatalysis.

Table 3. Comparison of Electrocatalytic Parameters for Electrocatalytic O_2 Reduction by Cobalt and Iron Complexes with Quinolic and Phenolic Ligands[a]

complex	$E_{1/2}$ for M(III/II)(V vs $Fc^{+/0}$)	η_{eff} (V)	TOF_{max} (s^{-1})	yield H_2O (%)[b]	ref
$[Co^{II}(Hqp1)](OTf)_2$ (**10**)	−0.49	0.33[c]	0.31[c]	61[c]	4
$[Co^{II}(Hpp1)](OTf)_2$ (**11**)	−0.47	0.31[c]	0.32[c]	11[c]	4
$[Fe^{II}(H_2qp1)](OTf)_2$ (**12**)	−0.26	inactive			88
$[Fe^{II}(H_4qp2)](OTf)_2$ (**13**)	−0.67	0.58	14.6	92	88
$[Fe^{II}(H_2qp3)](OTf)_2$ (**14**)	−0.56	0.42	3.3	83	88
$[Fe^{III}(H_4qp2)](OTf)_3$ (**15**)	−0.56	could not be determined (see text)			88
$[Fe^{III}(H_2qp3)](OTf)_3$ (**16**)	−0.56	0.37	3.2	81	88
$[Fe^{II}(Hpp3)](OTf)_2$ (**17**)	−0.52	0.41	N.D.	26	88

[a]All data were acquired in acetonitrile (MeCN) under N_2 with 100 mM $TBAPF_6$ as a supporting electrolyte and 50 mM AcOH/50 mM tetrabutylammonium acetate buffer. [b]Percent yield calculated from rotating ring-disk electrode (RRDE) measurements. [c]Electrocatalysis done with 1.0 mM catalyst and 50 mM AcOH/50 mM NaOAc.

https://doi.org/10.1021/acs.accounts.4c00645
Acc. Chem. Res. 2025, 58, 101−112

Scheme 6. Proposed Mechanism of Electrocatalytic O_2 Reduction for Quinol Complexes[a]

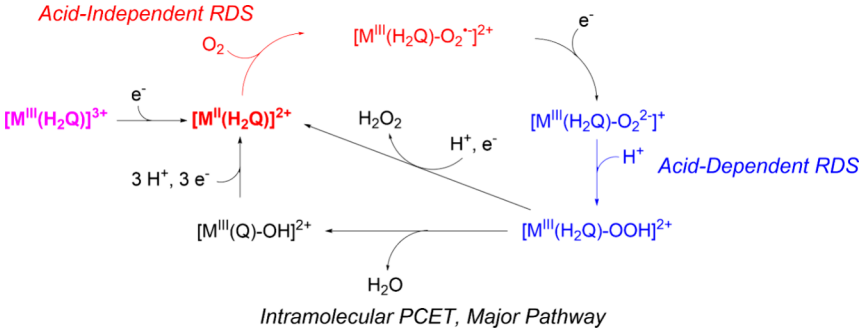

[a]Compounds **15** and **16** enter the cycle as M(III) species (purple). This graphic was adapted with permission from ref 88. Copyright 2024 American Chemical Society.

Thus far, the iron complexes differ from the cobalt electrocatalysts in that the phenol-for-quinol substitution impacts the rate of activity as well as the product selectivity.[4,88] Although **14** and its phenolic analog, $[Fe^{II}(Hpp1)](OTf)_2$ (**17**), have similar η_{eff} values, **17** is much less active, to the extent that TOF_{max} could not be reliably measured.[88] The ORR catalyzed by **17** is much less selective for water, which is reminiscent of the results for the cobalt-containing **10** and **11**.[4,88] Cobalt complexes with H_4qp2 and H_2qp3 are currently being investigated to determine whether these complexes are more active and selective for water than **14**.

The cobalt and iron complexes appear to proceed through fundamentally similar mechanisms (Scheme 6).[4,88] The identity of the rate-determining step (RDS) depends on the concentration of acid that is present. With low concentrations of acetic acid, the rate scales linearly with the concentration of acid, and the data are consistent with the protonation of a M(III)-superoxo species as the RDS. Notably, these complexes also exhibit minor ORR catalysis with no added acid, an observation attributed to the intramolecular proton transfer abilities of the quinolic groups. Moving further in the cycle, rapid electron electron and/or proton transfer from the quinol to the subsequent M(III)-OOH species is proposed to produce water. Alternatively, the HOO^- can be protonated to liberate H_2O_2. The higher water selectivity of **13** is proposed to be at least partly a consequence of its having a second quinol, although its higher η_{eff} would also be anticipated to favor water production.[88] With high amounts of acid, the rate no longer scales with the concentration of acid, and O_2 binding to M(II) species is instead proposed to be the RDS.[4,88] This step represents the effective upper-limit of ORR catalysis. An analysis of the TOF_0 (turnover frequency at zero overpotential) under the O_2 limiting conditions found **16** ($\log TOF_0 = -5.9$) to be the largest value reported for a homogeneous ORR electrocatalyst.[89−91]

5. CONCLUSION AND OUTLOOK

Installing quinols into polydentate organic ligands has thus far provided several catalytic benefits. With SOD and CAT mimics, the organic redox couples have supplemented and in some cases, replaced metal-based ones. The abilities of quinols to provide additional electrons beyond what a redox-active metal ion can provide has improved the product selectivity of cobalt- and iron-catalyzed oxygen reduction by facilitating the four-electron reduction of O_2 to water. The quinols have also enabled previously inactive pyridylamine ligands to promote electrocatalysis. The SOD, CAT, and ORR activities are strongly influenced by the ligand structure, and future work in these fields will focus on more clearly delineating these structure−function relationships in order to optimize catalytic activity.

AUTHOR INFORMATION

Corresponding Authors

Byron H. Farnum − *Department of Chemistry and Biochemistry, Auburn University, Auburn, Alabama 36849, United States;* orcid.org/0000-0001-9152-1909; Email: farnum@auburn.edu

Christian R. Goldsmith − *Department of Chemistry and Biochemistry, Auburn University, Auburn, Alabama 36849, United States;* orcid.org/0000-0001-7293-1267; Email: crgoldsmith@auburn.edu

Complete contact information is available at: https://pubs.acs.org/10.1021/acs.accounts.4c00645

Author Contributions

C.R.G. organized, wrote, and edited portions of the manuscript. B.H.F. wrote and edited portions of the manuscript.

Notes

The authors declare no competing financial interest.

Biographies

Byron H. Farnum is an Associate Professor of chemistry at Auburn University. He began his career at Auburn in 2016 after completing postdoctoral work with Prof. Thomas J. Meyer at the University of North Carolina at Chapel Hill. He received his Ph.D. (2012) from the Johns Hopkins University in the research group of Prof. Gerald J. Meyer. His research interests lie in the area of multielectron transfer reactions in single-metal complexes with applications in energy storage and catalysis.

Christian R. Goldsmith has been a Professor of chemistry at Auburn University since 2007 and was promoted to full professor in 2021. He received his Ph.D. (2004) from Stanford University under the direction of Prof. T. Daniel P. Stack and pursued postdoctoral studies at the Massachusetts Institute of Technology under the direction of Prof. Stephen J. Lippard (2004−2007). His research focuses on the synthesis and characterization of first-row transition metal complexes with redox-active organic ligands.

ACKNOWLEDGMENTS

We thank our collaborators and colleagues for their hard and meticulous work on these projects. We would like to especially

thank Prof. Ivana Ivanović-Burmazović and her research team at Ludwig-Maximilians-Universität München. The research described here was financially supported by Auburn University and the National Science Foundation (NSF-CHE-1662875 and NSF-CHE-1954336).

REFERENCES

(1) Senft, L.; Moore, J. L.; Franke, A.; Fisher, K. R.; Scheitler, A.; Zahl, A.; Puchta, R.; Fehn, D.; Ison, S.; Sader, S.; Ivanović-Burmazović, I.; Goldsmith, C. R. Quinol-Containing Ligands Enable High Superoxide Dismutase Activity by Modulating Coordination Number, Charge, Oxidation States and Stability of Manganese Complexes throughout Redox Cycling. *Chem. Sci.* **2021**, *12* (31), 10483−10500.
(2) Ward, M. B.; Scheitler, A.; Yu, M.; Senft, L.; Zillmann, A. S.; Gorden, J. D.; Schwartz, D. D.; Ivanović-Burmazović, I.; Goldsmith, C. R. Superoxide Dismutase Activity Enabled by a Redox-Active Ligand rather than Metal. *Nat. Chem.* **2018**, *10* (12), 1207−1212.
(3) Karbalaei, S.; Franke, A.; Oppelt, J.; Aziz, T.; Jordan, A.; Pokkuluri, P. R.; Schwartz, D. D.; Ivanović-Burmazović, I.; Goldsmith, C. R. A Macrocyclic Quinol-Containing Ligand Enables High Catalase Activity even with a Redox-Inactive Metal at the Expense of the Ability to Mimic Superoxide Dismutase. *Chem. Sci.* **2023**, *14* (36), 9910−9922.
(4) Obisesan, S. V.; Rose, C.; Farnum, B. H.; Goldsmith, C. R. Co(II) Complex with a Covalently Attached Pendent Quinol Selectively Reduces O_2 to H_2O. *J. Am. Chem. Soc.* **2022**, *144* (50), 22826−22830.
(5) Pahl, H. L.; Baeuerle, P. A. Oxygen and the Control of Gene Expression. *Bioessays* **1994**, *16* (7), 497−502.
(6) Armstrong, D. A.; Huie, R. E.; Koppenol, W. H.; Lymar, S. V.; Merényi, G.; Neta, P.; Ruscic, B.; Stanbury, D. M.; Steenken, S.; Wardman, P. Standard Electrode Potentials Involving Radicals in Aqueous Solution: Inorganic Radicals (IUPAC Technical Report). *Pure Appl. Chem.* **2015**, *87* (11−12), 1139−1150.
(7) Roberts, C. K.; Sindhu, K. K. Oxidative Stress and Metabolic Syndrome. *Life Sci.* **2009**, *84* (21-22), 705−712.
(8) Fearon, I. M.; Faux, S. P. Oxidative Stress and Cardiovascular Disease: Novel Tools Give (Free) Radical Insight. *J. Mol. Cell. Cardiol.* **2009**, *47* (3), 372−381.
(9) Eskici, G.; Axelsen, P. H. Copper and Oxidative Stress in the Pathogenesis of Alzheimer's Disease. *Biochemistry* **2012**, *51* (32), 6289−6311.
(10) Sheng, Y.; Abreu, I. A.; Cabelli, D. E.; Maroney, M. J.; Miller, A.-F.; Teixeira, M.; Valentine, J. S. Superoxide Dismutases and Superoxide Reductases. *Chem. Rev.* **2014**, *114* (7), 3854−3918.
(11) Zamocky, M.; Furtmüller, P. G.; Obinger, C. Evolution of Catalases from Bacteria to Humans. *Antioxid. Redox Signal.* **2008**, *10* (9), 1527−1548.
(12) Batinic-Haberle, I.; Reboucas, J. S.; Spasojevic, I. Superoxide Dismutase Mimics: Chemistry, Pharmacology, and Therapeutic Potential. *Antioxid. Redox Signal.* **2010**, *13* (6), 877−918.
(13) Tovmasyan, A.; Carballal, S.; Ghazaryan, R.; Melikyan, L.; Weitner, T.; Maia, C. G. C.; Reboucas, J. S.; Radi, R.; Spasojevic, I.; Benov, L.; Batinic-Haberle, I. Rational Design of Superoxide Dismutase (SOD) Mimics: The Evaluation of the Therapeutic Potential of New Cationic Mn Porphyrins with Linear and Cyclic Substituents. *Inorg. Chem.* **2014**, *53* (21), 11467−11483.
(14) Tovmasyan, A.; Maia, C. G. C.; Weitner, T.; Carballal, S.; Sampaio, R. S.; Lieb, D.; Ghazaryan, R.; Ivanovic-Burmazovic, I.; Ferrer-Sueta, G.; Radi, R.; Reboucas, J. S.; Spasojevic, I.; Benov, L.; Batinic-Haberle, I. A Comprehensive Evaluation of Catalase-Like Activity of Different Classes of Redox-Active Therapeutics. *Free Radical Biol. Med.* **2015**, *86*, 308−321.
(15) Wu, A. J.; Penner-Hahn, J. E.; Pecoraro, V. L. Structural, Spectroscopic, and Reactivity Models for the Manganese Catalases. *Chem. Rev.* **2004**, *104* (2), 903−938.
(16) Vincent, A.; Thauvin, M.; Quévrain, E.; Mathieu, E.; Layani, S.; Seksik, P.; Batinic-Haberle, I.; Vriz, S.; Policar, C.; Delsuc, N. Evaluation of the Compounds Commonly Known as Superoxide Dismutase and Catalase Mimics in Cellular Models. *J. Inorg. Biochem.* **2021**, *219*, 111431.
(17) Freire, D. M.; Johnston, H. M.; Smith, K. J.; Pota, K.; Mekhail, M. A.; Kharel, S.; Green, K. N. Hydrogen Peroxide Disproportionation Activity Is Sensitive to Pyridine Substitutions on Manganese Catalysts Derived from 12-Membered Tetra-Aza Macrocyclic Ligands. *Inorg. Chem.* **2023**, *62* (39), 15842−15855.
(18) Mekhail, M. A.; Smith, K. J.; Freire, D. M.; Pota, K.; Nguyen, N.; Burnett, M. E.; Green, K. N. Increased Efficiency of a Functional SOD Mimic Achieved with Pyridine Modification on a Pyclen-Based Copper(II) Complex. *Inorg. Chem.* **2023**, *62* (14), 5415−5425.
(19) Mahammed, A.; Gross, Z. Highly Efficient Catalase Activity of Metallocorroles. *Chem. Commun.* **2010**, *46* (37), 7040−7042.
(20) Friedel, F. C.; Lieb, D.; Ivanović-Burmazović, I. Comparative Studies on Manganese-Based SOD Mimetics, Including the Phosphate Effect, by Using Global Spectral Analysis. *J. Inorg. Biochem.* **2012**, *109*, 26−32.
(21) Gelasco, A.; Bensiek, S.; Pecoraro, V. L. The $[Mn_2(2\text{-}OHsalpn)_2]^{2-,1-,0}$ System: An Efficient Functional Model for the Reactivity and Inactivation of the Manganese Catalases. *Inorg. Chem.* **1998**, *37* (13), 3301−3309.
(22) Signorella, S.; Rompel, A.; Buldt-Karentzopoulos, K.; Krebs, B.; Pecoraro, V. L.; Tuchagues, J.-P. Reevaluation of the Kinetics of Polynuclear Mimics for Manganese Catalases. *Inorg. Chem.* **2007**, *46* (25), 10864−10868.
(23) Bonetta, R. Potential Therapeutic Applications of MnSODs and SOD-Mimetics. *Chem.—Eur. J.* **2018**, *24* (20), 5032−5041.
(24) Aston, K.; Rath, N.; Naik, A.; Slomczynska, U.; Schall, O. F.; Riley, D. P. Computer-Aided Design (CAD) of Mn(II) Complexes: Superoxide Dismutase Mimetics with Catalytic Activity Exceeding the Native Enzyme. *Inorg. Chem.* **2001**, *40* (8), 1779−1789.
(25) Riley, D. P. Functional Mimics of Superoxide Dismutase Enzymes as Therapeutic Agents. *Chem. Rev.* **1999**, *99* (9), 2573−2588.
(26) Riley, D. P.; Lennon, P. J.; Neumann, W. L.; Weiss, R. H. Toward the Rational Design of Superoxide Dismutase Mimics: Mechanistic Studies for the Elucidation of Substituent Effects on the Catalytic Activity of Macrocyclic Manganese(II) Complexes. *J. Am. Chem. Soc.* **1997**, *119* (28), 6522−6528.
(27) Riley, D. P.; Weiss, R. H. Manganese Macrocyclic Ligand Complexes as Mimics of Superoxide Dismutase. *J. Am. Chem. Soc.* **1994**, *116* (1), 387−388.
(28) Ching, H. Y. V.; Kenkel, I.; Delsuc, N.; Mathieu, E.; Ivanović-Burmazović, I.; Policar, C. Bioinspired Superoxide-Dismutase Mimics: The Effects of Functionalization with Cationic Polyarginine Peptides. *J. Inorg. Biochem.* **2016**, *160*, 172−179.
(29) Lieb, D.; Friedel, F. C.; Yawer, M.; Zahl, A.; Khusniyarov, M. M.; Heinemann, F. W.; Ivanović-Burmazović, I. Dinuclear Seven-Coordinate Mn(II) Complexes: Effect of Manganese(II)-Hydroxo Species on Water Exchange and Superoxide Dismutase Activity. *Inorg. Chem.* **2013**, *52* (1), 222−236.
(30) Liu, G.-F.; Dürr, K.; Puchta, R.; Heinemann, F. W.; van Eldik, R.; Ivanović-Burmazović, I. Chelate Electronic Properties Control the Redox Behaviour and Superoxide Reactivity of Seven-Coordinate Manganese(II) Complexes. *Dalton Trans.* **2009**, No. 32, 6292−6295.
(31) Salvemini, D.; Wang, Z.-Q.; Zweier, J. L.; Samouilov, A.; Macarthur, H.; Misko, T. P.; Currie, M. G.; Cuzzocrea, S.; Sikorski, J. A.; Riley, D. P. A Nonpeptidyl Mimic of Superoxide Dismutase with Therapeutic Activity in Rats. *Science* **1999**, *286* (5438), 304−306.
(32) Batinic-Haberle, I.; Spasojevic, I. 25 Years of Development of Mn Porphyrins — from Mimics of Superoxide Dismutase Enzymes to Thiol Signaling to Clinical Trials: The Story of our Life in the USA. *J. Porphyr. Phthalocyanines* **2019**, *23* (11−12), 1326−1335.
(33) Batinić-Haberle, I.; Liochev, S. I.; Spasojević, I.; Fridovich, I. A Potent Superoxide Dismutase Mimic: Manganese β-Octabromo-meso-tetrakis-(N-methylpyridinium-4-yl) Porphyrin. *Arch. Biochem. Biophys.* **1997**, *343* (2), 225−233.
(34) Batinic-Haberle, I.; Tovmasyan, A.; Spasojevic, I. Mn Porphyrin-Based Redox-Active Drugs: Differential Effects as Cancer Therapeutics

https://doi.org/10.1021/acs.accounts.4c00645
Acc. Chem. Res. 2025, 58, 101−112

and Protectors of Normal Tissue Against Oxidative Injury. *Antioxid. Redox Signal.* **2018**, *29* (16), 1691−1724.
(35) Freire, D. M.; Beeri, D.; Pota, K.; Johnston, H. M.; Palacios, P.; Pierce, B. S.; Sherman, B. D.; Green, K. N. Hydrogen Peroxide Disproportionation with Manganese Macrocyclic Complexes of Cyclen and Pyclen. *Inorg. Chem. Front.* **2020**, *7* (7), 1573−1582.
(36) Adam, S. M.; Wijeratne, G. B.; Rogler, P. J.; Diaz, D. E.; Quist, D. A.; Liu, J. J.; Karlin, K. D. Synthetic Fe/Cu Complexes: Toward Understanding Heme-Copper Oxidase Structure and Function. *Chem. Rev.* **2018**, *118* (22), 10840−11022.
(37) Wikström, M.; Krab, K.; Sharma, V. Oxygen Activation and Energy Conservation by Cytochrome c Oxidase. *Chem. Rev.* **2018**, *118* (5), 2469−2490.
(38) Yoshikawa, S.; Shimada, A. Reaction Mechanism of Cytochrome c Oxidase. *Chem. Rev.* **2015**, *115* (4), 1936−1989.
(39) Sun, Y.; Sinev, I.; Ju, W.; Bergmann, A.; Dresp, S.; Kühl, S.; Spöri, C.; Schmies, H.; Wang, H.; Bernsmeier, D.; Paul, B.; Schmack, R.; Kraehnert, R.; Roldan Cuenya, B.; Strasser, P. Efficient Electrochemical Hydrogen Peroxide Production from Molecular Oxygen on Nitrogen-Doped Mesoporous Carbon Catalysts. *ACS Catal.* **2018**, *8* (4), 2844−2856.
(40) Mase, K.; Yoneda, M.; Yamada, Y.; Fukuzumi, S. Seawater Usable for Production and Consumption of Hydrogen Peroxide as a Solar Fuel. *Nat. Commun.* **2016**, *7* (1), 11470.
(41) Fukuzumi, S. Production of Liquid Solar Fuels and Their Use in Fuel Cells. *Joule* **2017**, *1* (4), 689−738.
(42) Miglbauer, E.; Wójcik, P. J.; Głowacki, E. D. Single-Compartment Hydrogen Peroxide Fuel Cells with Poly(3,4-ethylenedioxythiophene) Cathodes. *Chem. Commun.* **2018**, *54* (84), 11873−11876.
(43) Gasteiger, H. A.; Kocha, S. S.; Sompalli, B.; Wagner, F. T. Activity Benchmarks and Requirements for Pt, Pt-Alloy, and Non-Pt Oxygen Reduction Catalysts for PEMFCs. *Appl. Catal., B* **2005**, *56* (1), 9−35.
(44) Solomon, E. I.; Stahl, S. S. Introduction: Oxygen Reduction and Activation in Catalysis. *Chem. Rev.* **2018**, *118* (5), 2299−2301.
(45) Shao, M.; Chang, Q.; Dodelet, J.-P.; Chenitz, R. Recent Advances in Electrocatalysts for Oxygen Reduction Reaction. *Chem. Rev.* **2016**, *116* (6), 3594−3657.
(46) Machan, C. W. Advances in the Molecular Catalysis of Dioxygen Reduction. *ACS Catal.* **2020**, *10* (4), 2640−2655.
(47) Pegis, M. L.; Wise, C. F.; Martin, D. J.; Mayer, J. M. Oxygen Reduction by Homogeneous Molecular Catalysts and Electrocatalysts. *Chem. Rev.* **2018**, *118* (5), 2340−2391.
(48) Costentin, C.; Dridi, H.; Savéant, J.-M. Molecular Catalysis of O_2 Reduction by Iron Porphyrins in Water: Heterogeneous versus Homogeneous Pathways. *J. Am. Chem. Soc.* **2015**, *137* (42), 13535−13544.
(49) Martin, D. J.; Mayer, J. M. Oriented Electrostatic Effects on O_2 and CO_2 Reduction by a Polycationic Iron Porphyrin. *J. Am. Chem. Soc.* **2021**, *143* (30), 11423−11434.
(50) Brezny, A. C.; Johnson, S. I.; Raugei, S.; Mayer, J. M. Selectivity-Determining Steps in O_2 Reduction Catalyzed by Iron(tetramesitylporphyrin). *J. Am. Chem. Soc.* **2020**, *142* (9), 4108−4113.
(51) Singha, A.; Mondal, A.; Nayek, A.; Dey, S. G.; Dey, A. Oxygen Reduction by Iron Porphyrins with Covalently Attached Pendent Phenol and Quinol. *J. Am. Chem. Soc.* **2020**, *142* (52), 21810−21828.
(52) Wang, Y.-H.; Pegis, M. L.; Mayer, J. M.; Stahl, S. S. Molecular Cobalt Catalysts for O_2 Reduction: Low-Overpotential Production of H_2O_2 and Comparison with Iron-Based Catalysts. *J. Am. Chem. Soc.* **2017**, *139* (46), 16458−16461.
(53) Nichols, A. W.; Cook, E. N.; Gan, Y. J.; Miedaner, P. R.; Dressel, J. M.; Dickie, D. A.; Shafaat, H. S.; Machan, C. W. Pendent Relay Enhances H_2O_2 Selectivity during Dioxygen Reduction Mediated by Bipyridine-Based Co-N_2O_2 Complexes. *J. Am. Chem. Soc.* **2021**, *143* (33), 13065−13073.
(54) Wang, Y.-H.; Goldsmith, Z. K.; Schneider, P. E.; Anson, C. W.; Gerken, J. B.; Ghosh, S.; Hammes-Schiffer, S.; Stahl, S. S. Kinetic and Mechanistic Characterization of Low-Overpotential, H_2O_2-Selective Reduction of O_2 Catalyzed by N_2O_2-Ligated Cobalt Complexes. *J. Am. Chem. Soc.* **2018**, *140* (34), 10890−10899.
(55) Chlistunoff, J.; Sansiñena, J.-M. Effects of Axial Coordination of the Metal Center on the Activity of Iron Tetraphenylporphyrin as a Nonprecious Catalyst for Oxygen Reduction. *J. Phys. Chem. C* **2014**, *118* (33), 19139−19149.
(56) Kobayashi, N.; Nishiyama, Y. Catalytic Electroreduction of Molecular Oxygen using Iron or Cobalt 4,4',4'',4'''-Tetracarboxyphthalocyanine. *J. Phys. Chem.* **1985**, *89* (7), 1167−1170.
(57) Wang, Y.-H.; Schneider, P. E.; Goldsmith, Z. K.; Mondal, B.; Hammes-Schiffer, S.; Stahl, S. S. Brønsted Acid Scaling Relationships Enable Control Over Product Selectivity from O_2 Reduction with a Mononuclear Cobalt Porphyrin Catalyst. *ACS Cent. Sci.* **2019**, *5* (6), 1024−1034.
(58) Dong, Y.; Lv, X.; Sun, Y.; Zhao, Q.; Lei, H.; Wu, F.; Zhang, T.; Xue, Z.; Cao, R.; Qiu, F.; Xue, S. Electrocatalytic Oxygen Reduction Reaction of Peripheral Functionalized Cobalt Porphyrins(2.1.2.1). *Inorg. Chem.* **2024**, *63* (11), 4797−4801.
(59) Wang, Y.-H.; Mondal, B.; Stahl, S. S. Molecular Cobalt Catalysts for O_2 Reduction to H_2O_2: Benchmarking Catalyst Performance via Rate-Overpotential Correlations. *ACS Catal.* **2020**, *10* (20), 12031−12039.
(60) Liu, T.; Qin, H.; Xu, Y.; Peng, X.; Zhang, W.; Cao, R. Steric Effects on the Oxygen Reduction Reaction with Cobalt Porphyrin Atropisomers. *ACS Catal.* **2024**, *14* (9), 6644−6649.
(61) Nichols, A. W.; Kuehner, J. S.; Huffman, B. L.; Miedaner, P. R.; Dickie, D. A.; Machan, C. W. Reduction of Dioxygen to Water by a Co(N_2O_2) Complex with a 2,2′-Bipyridine Backbone. *Chem. Commun.* **2021**, *57* (4), 516−519.
(62) Cook, E. N.; Dickie, D. A.; Machan, C. W. Catalytic Reduction of Dioxygen to Water by a Bioinspired Non-Heme Iron Complex via a 2 + 2 Mechanism. *J. Am. Chem. Soc.* **2021**, *143* (40), 16411−16418.
(63) Passard, G.; Ullman, A. M.; Brodsky, C. N.; Nocera, D. G. Oxygen Reduction Catalysis at a Dicobalt Center: The Relationship of Faradaic Efficiency to Overpotential. *J. Am. Chem. Soc.* **2016**, *138* (9), 2925−2928.
(64) Han, J.; Tan, H.; Guo, K.; Lv, H.; Peng, X.; Zhang, W.; Lin, H.; Apfel, U.-P.; Cao, R. The "Pull Effect" of a Hanging Zn^{II} on Improving the Four-Electron Oxygen Reduction Selectivity with Co Porphyrin. *Angew. Chem., Int. Ed.* **2024**, *63* (36), e202409793.
(65) Song, Y.; Buettner, G. R. Thermodynamic and Kinetic Considerations for the Reaction of Semiquinone Radicals to Form Superoxide and Hydrogen Peroxide. *Free Radical Biol. Med.* **2010**, *49* (6), 919−962.
(66) Trumpower, B. L. The Protonmotive Q Cycle. Energy Transduction by Coupling of Proton Translocation to Electron Transfer by the Cytochrome bc1 Complex. *J. Biol. Chem.* **1990**, *265* (20), 11409−11412.
(67) Tiemann, R.; Renger, G.; Gräber, P.; Witt, H. T. The Plastoquinone Pool as Possible Hydrogen Pump in Photosynthesis. *Biochim. Biophys. Acta* **1979**, *546* (3), 498−519.
(68) Anson, C. W.; Stahl, S. S. Cooperative Electrocatalytic O_2 Reduction Involving Co(salophen) with *p*-Hydroquinone as an Electron-Proton Transfer Mediator. *J. Am. Chem. Soc.* **2017**, *139* (51), 18472−18475.
(69) Hooe, S. L.; Rheingold, A. L.; Machan, C. W. Electrocatalytic Reduction of Dioxygen to Hydrogen Peroxide by a Molecular Manganese Complex with a Bipyridine-Containing Schiff Base Ligand. *J. Am. Chem. Soc.* **2018**, *140* (9), 3232−3241.
(70) Horak, K. T.; Agapie, T. Dioxygen Reduction by a Pd(0)-Hydroquinone Diphosphine Complex. *J. Am. Chem. Soc.* **2016**, *138* (10), 3443−3452.
(71) Verboom, R. C.; Plietker, B. J.; Bäckvall, J.-E. New Chiral Diamide Ligands Containing Redox-Active Hydroquinone Groups. Synthesis and Results in the Palladium(II)-Catalyzed 1,4-Diacetoxylation of 1,3-Dienes. *J. Organomet. Chem.* **2003**, *687* (2), 508−517.
(72) Costentin, C.; Robert, M.; Savéant, J.-M. Current Issues in Molecular Catalysis Illustrated by Iron Porphyrins as Catalysts of the CO_2-to-CO Electrochemical Conversion. *Acc. Chem. Res.* **2015**, *48* (12), 2996−3006.

https://doi.org/10.1021/acs.accounts.4c00645
Acc. Chem. Res. 2025, 58, 101−112

(73) Karbalaei, S.; Franke, A.; Jordan, A.; Rose, C.; Pokkuluri, P. R.; Beyers, R. J.; Zahl, A.; Ivanović-Burmazović, I.; Goldsmith, C. R. A Highly Water- and Air-Stable Iron-Containing MRI Contrast Agent Sensor for H_2O_2. *Chem.—Eur. J.* **2022**, *28* (46), e202201179.
(74) Karbalaei, S.; Knecht, E.; Franke, A.; Zahl, A.; Saunders, A. C.; Pokkuluri, P. R.; Beyers, R. J.; Ivanović-Burmazović, I.; Goldsmith, C. R. A Macrocyclic Ligand Framework That Improves Both the Stability and T_1-Weighted MRI Response of Quinol-Containing H_2O_2 Sensors. *Inorg. Chem.* **2021**, *60* (12), 8368−8379.
(75) Yu, M.; Ambrose, S. L.; Whaley, Z. L.; Fan, S.; Gorden, J. D.; Beyers, R. J.; Schwartz, D. D.; Goldsmith, C. R. A Mononuclear Manganese(II) Complex Demonstrates a Strategy to Simultaneously Image and Treat Oxidative Stress. *J. Am. Chem. Soc.* **2014**, *136* (37), 12836−12839.
(76) Yu, M.; Ward, M. B.; Franke, A.; Ambrose, S. L.; Whaley, Z. L.; Bradford, T. M.; Gorden, J. D.; Beyers, R. J.; Cattley, R. C.; Ivanović-Burmazović, I.; Schwartz, D. D.; Goldsmith, C. R. Adding a Second Quinol to a Redox-Responsive MRI Contrast Agent Improves Its Relaxivity Response to H_2O_2. *Inorg. Chem.* **2017**, *56* (5), 2812−2826.
(77) Batinic-Haberle, I.; Rajic, Z.; Tovmasyan, A.; Reboucas, J. S.; Ye, X.; Leong, K. W.; Dewhirst, M. W.; Vujaskovic, Z.; Benov, L.; Spasojevic, I. Diverse Functions of Cationic Mn(III) N-substituted Pyridylporphyrins, Recognized as SOD Mimics. *Free Radical Biol. Med.* **2011**, *51* (5), 1035−1053.
(78) Aitken, J. B.; Shearer, E. L.; Giles, N. M.; Lai, B.; Vogt, S.; Reboucas, J. S.; Batinic-Haberle, I.; Lay, P. A.; Giles, G. I. Intracellular Targeting and Pharmacological Activity of the Superoxide Dismutase Mimics MnTE-2-PyP^{5+} and MnTnHex-2-PyP^{5+} Regulated by Their Porphyrin Ring Substituents. *Inorg. Chem.* **2013**, *52* (8), 4121−4123.
(79) Miller, A.-F. Redox Tuning over Almost 1 V in a Structurally Conserved Active Site: Lessons from Fe-Containing Superoxide Dismutase. *Acc. Chem. Res.* **2008**, *41* (4), 501−510.
(80) Iranzo, O. Manganese Complexes Displaying Superoxide Dismutase Activity: A Balance between Different Factors. *Bioorg. Chem.* **2011**, *39* (2), 73−87.
(81) McCord, J. M.; Fridovich, I. Superoxide Dismutase: An Enzymic Function for Erythrocuprein (Hemocuprein). *J. Biol. Chem.* **1969**, *244* (22), 6049−6055.
(82) Kenkel, I.; Franke, A.; Dürr, M.; Zahl, A.; Dücker-Benfer, C.; Langer, J.; Filipović, M. R.; Yu, M.; Puchta, R.; Fiedler, S. R.; Shores, M. P.; Goldsmith, C. R.; Ivanović-Burmazović, I. Switching between Inner- and Outer-Sphere PCET Mechanisms of Small-Molecule Activation: Superoxide Dismutation and Oxygen/Superoxide Reduction Reactivity Deriving from the Same Manganese Complex. *J. Am. Chem. Soc.* **2017**, *139* (4), 1472−1484.
(83) Moore, J. L.; Oppelt, J.; Senft, L.; Franke, A.; Scheitler, A.; Dukes, M. W.; Alix, H. B.; Saunders, A. C.; Karbalaei, S.; Schwartz, D. D.; Ivanović-Burmazović, I.; Goldsmith, C. R. Diquinol Functionality Boosts the Superoxide Dismutase Mimicry of a Zn(II) Complex with a Redox-Active Ligand while Maintaining Catalyst Stability and Enhanced Activity in Phosphate Solution. *Inorg. Chem.* **2022**, *61* (49), 19983−19997.
(84) Miliordos, E.; Moore, J. L.; Obisesan, S. V.; Oppelt, J.; Ivanović-Burmazović, I.; Goldsmith, C. R. Computational Analysis of the Superoxide Dismutase Mimicry Exhibited by a Zinc(II) Complex with a Redox-Active Organic Ligand. *J. Phys. Chem. A* **2024**, *128* (8), 1491−1500.
(85) Swallow, A. J. In *Functions of Quinones in Energy Converting Systems*, Trumpower, B. L., Ed.; Elsevier, Inc., 1982; pp 59−72.
(86) Zhao, X.; Imahori, H.; Zhan, C.-G.; Sakata, Y.; Iwata, S.; Kitagawa, T. Resonance Raman and FTIR Spectra of Isotope-Labeled Reduced 1,4-Benzoquinone and Its Protonated Forms in Solutions. *J. Phys. Chem. A* **1997**, *101* (4), 622−631.
(87) Haber, A.; Gross, Z. Catalytic Antioxidant Therapy by Metallodrugs: Lessons from Metallocorroles. *Chem. Commun.* **2015**, *51* (27), 5812−5827.
(88) Obisesan, S. V.; Parvin, M.; Tao, M.; Ramos, E.; Saunders, A. C.; Farnum, B. H.; Goldsmith, C. R. Installing Quinol Proton/Electron Mediators onto Non-Heme Iron Complexes Enables Them to Electrocatalytically Reduce O_2 to H_2O at High Rates and Low Overpotentials. *Inorg. Chem.* **2024**, *63* (30), 14126−14141.
(89) Pegis, M. L.; McKeown, B. A.; Kumar, N.; Lang, K.; Wasylenko, D. J.; Zhang, X. P.; Raugei, S.; Mayer, J. M. Homogenous Electrocatalytic Oxygen Reduction Rates Correlate with Reaction Overpotential in Acidic Organic Solutions. *ACS Cent. Sci.* **2016**, *2* (11), 850−856.
(90) Martin, D. J.; Mercado, B. Q.; Mayer, J. M. Combining Scaling Relationships Overcomes Rate versus Overpotential Trade-Offs in O_2 Molecular Electrocatalysis. *Sci. Adv.* **2020**, *6* (11), eaaz3318.
(91) Bhunia, S.; Ghatak, A.; Rana, A.; Dey, A. Amine Groups in the Second Sphere of Iron Porphyrins Allow for Higher and Selective $4e^-/4H^+$ Oxygen Reduction Rates at Lower Overpotentials. *J. Am. Chem. Soc.* **2023**, *145* (6), 3812−3825.

https://doi.org/10.1021/acs.accounts.4c00645
Acc. Chem. Res. 2025, 58, 101−112